From PbI_2 to $MAPbI_3$ through Layered Intermediates

Giovanna Pellegrino[1], Stefania D'Angelo[2], Ioannis Deretzis[1], Guglielmo Guido Condorelli[2], Emanuele Smecca[1], Graziella Malandrino[2], Antonino La Magna[1]and Alessandra Alberti[1*]

[1] CNR-IMM Zona Industriale, VIII Strada, No. 5, 95121 Catania, Italy

[2] Dipartimento Scienze Chimiche, Università degli studi di Catania and INSTM UdR Catania, V.le A. Doria 6, 95125 Catania, Italy

ABSTRACT

In the present work, we describe the process of formation of methyl ammonium lead iodide perovskite ($MAPbI_3$) by reaction between [001] oriented PbI_2 thin films and MAI. The reaction leads to a rapid change in the optical properties with the formation of a brown phase having a large band in the visible range and a contribution in the near- UV range (375 nm). X-ray Diffraction analyses indicate that the MAI+PbI_2 as-obtained material mainly consists of a highly oriented matrix of MAI that intermixes with the Pb-I precursor. A chemical exfoliation of the initial PbI_2 structure with the massive intercalation of the methyl-ammonium iodide ions suitably describes the optical and structural findings. Short thermally treating (100°C) of this as-obtained sample results in the formation of a second oriented intermediate phase, attributed to the presence of a low-dimensional perovskite structure. Such low-dimensional metastable phase is no longer visible by increasing the annealing time or the annealing temperature (150°C), with the single 3D $MAPbI_3$ tetragonal phase present in the XRD pattern.

INTRODUCTION

In the last years, organic/inorganic hybrid perovskites have encountered remarkable attention within the scientific community for their attractive properties which find applications in the opto-electronic devices and solar cells.[1,2]

The first results in the field of photovoltaics (PV) were published in 2009 by Miyasaka's group which reports on the sensitization of mesoporous TiO_2 films by two different types of organo-lead halide perovskite nanocrystals, namely methyl-ammonium lead bromide ($CH_3NH_3PbBr_3$) and iodide($CH_3NH_3PbI_3$).[3] From that date, in a short lapse of time, the use of organo/lead/halide- based materials as solid state heterojunction has registered improving performances and efficiencies nowadays comparable to those of silicon.[4]

More recently, near-infrared photoemission and electro-luminescence properties of the hybrid halide perovskite have found application as light-emitting compounds and as sensitive components in photo-detectors.[5-8]

The conspicuous interest towards the family of organic/ halide perovskites is mainly due to the unusual combination of properties typically belonging to both the molecular compounds (optical tunability, highlight-absorbing coefficient, easy and cheap manufacturing) and to the inorganic semiconductors (robustness, high charge transport character and diffusion lengths).[9,10]

The versatility of the hybrid perovskite engineering is demonstrated by the huge number of works in literature. Such variability is mainly due to the easy synthetic interchange of the metal, the organic cation and the halide anion, to obtain a final material with controlled absorption and charge transport characteristics. For example, the band gap of $CH_3NH_3PbI_3$ can be tailored by replacing the methylammonium cation (MA^+) with the slightly larger formamidinium cation ($H_2N\text{-}CH{=}NH_2$)[11] or by chemically managing the Br-content.[12]

Besides that, also the stoichiometric proportion between the elements and the consequent structural atomic arrangement becomes a crucial aspect for the characteristics of the final material. In the large family of organo lead-iodide-based perovskites, in fact, the $[PbI_6]^{4-}$ units can form three-dimensional (3-D), two-dimensional (2-D),one-dimensional (1-D) or zero-dimensional (0-D) networks, depending on the sharing of the iodine at the corners of the octahedral units. The n-D architectures have different stoichiometry, crystallographic habits and optical properties.[13]

In particular, the three-dimensional (3D) lattices consist of networks of all corner-connected octahedra extended along the three spatial coordinates with the small organic ammonium moiety (e.g. $CH_3NH_3^+$, $HC(NH_2)_2^+$) filling the holes between the octahedra. In the case of $MAPbI_3$, for instance, the structure shows the I4-mcm tetragonal symmetry with a=b=8.86 Å and c=12.64 Å.[18] Two main methods are reported in literature for the synthesis of the $MAPbI_3$ 3D perovskite, based on spin-coating and thermal evaporation of the MAI and PbI_2 precursors.[19-22] In particular, both the evaporation and the wet procedure can be performed by following a single step or sequential deposition. Very recently, Patel and al. reported on the dynamics of $MAPbI_3$ formation from the PbI_2 through the interaction with MAI by following a two- step thermal evaporation procedure. [23]

The two-dimensional (2D) lattices are self-organized layers formed from a simple intercalation of RNH_3^+ into the PbI_2 sheets to yield well-ordered films (quantum wells). [17,24,25] Such hybrid structures take the generic structural formula of A_2MX_4, where A is a primary (alkyl or aromatic) ammonium cation (RNH_3^+), M is a metal of the IV group and X a halogen. Such materials are known as monolayer perovskites, consisting of a single network of connected octahedral units sandwiched by frames of organic monoamine. The organic/inorganic alternate stacking is organized by attractive ionic interactions between the RNH_3^+ and PbI_6^{4-} whilst van der Waals interactions occurring within the organic chains of the molecular layer (spacer).This confines the perovskite in bi-dimensionality because of steric effects.

Nevertheless, the ammonium moieties in those structures present long alkyl chains which stabilize the organic framework by van der Waals interaction. In such lead/iodide-based 2D structures, the

lattice parameters $a = b$ are very similar, being in the range of 8.7÷9.0 Å [26,27].The value of the *c*-axis is, instead, related to the nature of the intercalated organic molecule. Interestingly, *a* and *b* parameters are very close to those belonging to the tetragonal $MAPbI_3$ phase.

The 2.5 dimensionality (2.5D) is also reported for perovskite.[28,29,30] Such hybrids structures contain a bilayer of inorganic network and take the generic formula $(A)_2(MA)Pb_2I_7$, with the presence of the MA moiety. [15]

Thanks to the reduced size of the MA^+ cation (small hindrance), this ion can be accommodated inside the lead-iodide inorganic network, occupying the same crystallographic position of that occurring in $MAPbI_3$. Structural similarities are, then, recognizable between the $(A)_2(MA)Pb_2I_7$ and the 3D arrangement [31] for the presence of MA^+ ion inside the lattice.

The variability of the organo/lead/iodide structures encourages a deep comprehension of the phenomena regarding the interaction between the two initial precursors PbI_2 and MAI. It is expected, for instance, that the small gas phase methylamine molecules and hydrogen iodide (HI) can intercalate in the sheet-like PbI_2 structure with relative easiness.[32]

In this paper, the interaction between PbI_2 and MAI through a chemical two step method is presented. To this purpose, simplified systems consisting of uniform PbI_2 thin layers (20 ±5 nm), grown [00l]-oriented on TiO_2 flat substrates were used. We analyzed the layers as-obtained by the PbI_2/MAI reaction at room temperature and after mild annealing processes. All the reactions and the thermal treatments, here described, have been carried out in inert atmosphere (H_2O, O_2< 1 ppm) to prevent contaminations and to avoid the effects attributable to the presence of water. We observed the formation of highly oriented MA/lead/iodide intermediate phases from PbI_2 as the result of the intercalation of the organic parts in the inorganic Pb-I framework. The approach described in the paper has allowed us to follow the steps of the initial interaction between the PbI_2 and MAI from the early stage. Phase modifications of the inorganic/organic self-assembled structures as induced by thermal treatments have been also discussed in the paper providing a detailed structural,

morphological and optical characterization of the organo/lead/iodide structures all along the phase-transformations.

EXPERIMENTAL SECTION

Preparation of TiO_2 layers

TiO_2 layers with a thickness of ~37 nm have been deposited on 1737 Corning glass (0.9 mm-thick, having Root Mean Square roughness (RMS) <0.5nm), by dc-reactive sputtering (Kenotec equipment) in O_2 ambient using a 6 inch titanium target plate having an effective 5 inch erosion zone. The process was carried out by applying a constant power of ~600W (1.24 A, 498V, power loading 4.9Wcm^{-2}) for 480 s, an O_2/Ar flow rate ratio as low as 5/45 sccm and by setting the external heater in such a way that the value measured on the sample surface was~150 °C. Sputtering deposition guarantees a precise control over the thickness, roughness and uniformity of the deposited layers.

The samples have been annealed at 150°C for 30 minutes in order to remove the adsorbed water.

Reagents and solvents

MAI was purchased by Dyesol. PbI_2, anhydrous N,N-dimethylformamide (DMF, >99%) and anhydrous isopropyl alcohol (>99.7%) were purchased by Aldrich. All the products were opened and kept inside a Glove-box (O_2<1ppm, H_2O<1ppm), and used as received.

Preparation of PbI_2 layers

The deposition of PbI_2 on the TiO_2 substrates was performed inside a glove-box (O_2<1ppm, H_2O<1ppm) by using the following approach.

The thermally treated (150°C, 30 min) TiO_2 sample (0.5 cm x 2 cm) was positioned inside a home-made reactor to form the desired angle. The reactor is a vessel equipped with a funnel and a tap. The vessel was filled with a $5x10^{-2}$ M solution of PbI_2 in anhydrous DMF in such a way that the TiO_2 sample was almost completely covered. The elution of the PbI_2 solution on the TiO_2 surface is regulated by opening the orifice of the funnel (see the schematic in the inset of Figure 1). The control of its aperture is mandatory to guarantee a constant flow of the solution (10 ml/min) which is equal for all the sample preparations. This process has been baptized "Gravity Coating". The PbI_2/TiO_2 samples have been annealed at 100°C for 30 min in order to remove the solvent.

Reaction with MAI

Different concentrations of MAI solutions, namely $5x10^{-2}$ M, $1x10^{-2}$ M and $5x10^{-4}$M, were prepared inside the glove-box by using anhydrous isopropyl alcohol. The PbI_2 sample was immersed in the MAI solution for 10 min, removed from the solution and dried in N_2. The samples were analyzed as obtained and following thermal treatments at 100°C for different annealing times (30 and 180 min). A number of six samples have been prepared and investigated in order to have a large reliable statistics. The analyses followed immediately the preparation of the samples or after a relatively short lapse of time (<3h).

Characterization techniques

X-*ray Reflectivity*

X-ray Reflectivity (XRR) were carried out by using a D8-Discover Bruker AXS diffractometer equipped with a Cu X-ray source. The setup for the analysis consists of a Goebel mirror and 0.1 mm slits at the primary optics, 0.2 mm slits with a scintillator as detector at the secondary optics. The best fits for the XRR curves have been obtained by using the software LEPTOS 7.05 [https://www.bruker.com/products/x-ray-diffraction-and-elemental-analysis/x-ray-diffraction/xrd-software/overview/leptos.html] and a combination of Genetic Algorithm and Var-metrix/simplex

method. The parameters found for the TiO_2substrate have been adopted as invariable factors for the fitting of the profile of the PbI_2 /TiO_2 sample.

Atomic Force Microscopy

Atomic Force Microscopy (AFM) images were obtained in tapping mode by a NT-MDT instrument. The used frequency of the tips is in the range between 140÷170 kHz and the oscillation amplitude was set at 12 nm.

X-ray Diffraction

X-ray diffraction (XRD) analyses have been performed using a D8-Discover Bruker-AXS Diffractometer equipped with a Cu-kα X-ray source, a Goebel mirror and a thin film attachment. The XRD patterns were collected in symmetric configuration in the 2θ range 5÷36° by using a step of 0.02°. Rocking curves measurements were collected by using a step of 0.05°.

Uv-vis spectroscopy

These measurements were carried out by using a UV−vis V-650 Jasco spectrophotometer. The analyses were performed in the range between 350 and 900 nm, by using a step of and a of 400 nm/min.

RESULTS AND DISCUSSION

PbI_2 sample characterization

X-ray Reflectivity. Layers of PbI_2 have been deposited on TiO_2 films according to the procedure described in the experimental section. In order to provide information on the thickness, roughness and density of the obtained layers, X-ray reflectivity (XRR) analyses were performed by comparing the bare TiO_2 substrate and the PbI_2/TiO_2 bi-layer. The periodicity of the interference features (Kiessig fringes) found in the XRR curve is associated with the thickness of the layers, the slope of the curve with the roughness (scattering of the X-ray from the surface) and the position of the critical angle with the density of the films.

The XRR curves related to the TiO_2 sample before (—) and after (—) the process of PbI_2 deposition are shown in figure 1.

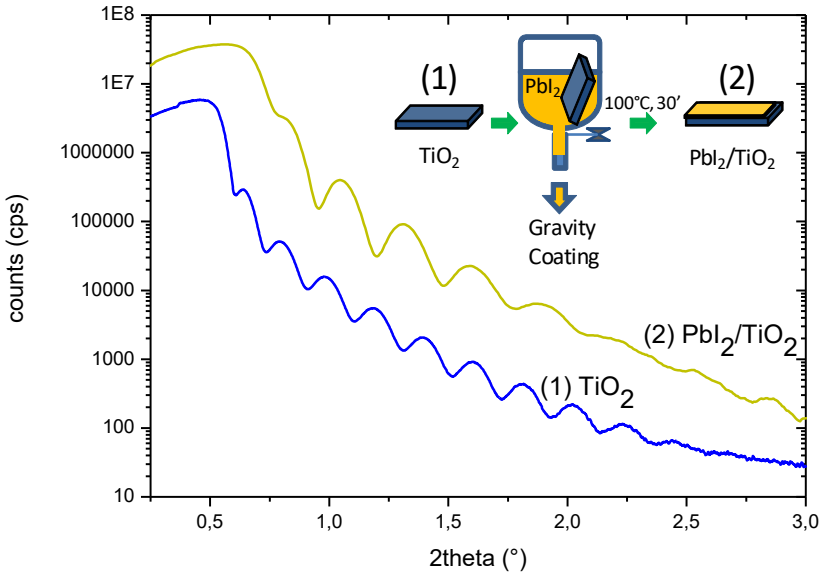

Figure 1 XRR profiles of 1)TiO_2 and 2)PbI_2/TiO_2 samples and, in the inset, the schematic representing the elution of PbI_2 on the TiO_2 substrate according to the "Gravity Coating" process described in the experimental section.

The best fit obtained for the XRR curve of theTiO_2sample indicates a thickness of ~38±5 nm, a roughness of ~2.8 nm and a density of ~3.7 g/cm^3, in line with what previously reported.[33,34] The value of the density, lower than that expected for the anatase polymorph (3.91 g/cm^3), is the result of the material nano- porosity, likely due to the deposition used procedure.[34]

After the deposition of PbI_2, the presence of an overlayer, affects the modulation of the Kiessig fringes in the XRR profile (figure 1—) and the slope of the curve. Additionally, the critical angle is shifted at higher 2θ values consistently with the presence of a material denser than TiO_2. For the fitting procedure, we keep constant the parameters found for TiO_2 layer. Correspondingly, the best fit for the experimental XRR curve of the PbI_2/TiO_2 bi-layer reveals a thickness of PbI_2 in the range of 20±5 nm, a roughness of ~7.5 nm and a density ~5.58 g/cm^3. Such density value is, again, lower

than that expected for PbI_2 (6.16 g/cm^3), thus suggesting the presence of a not compact layer. Further information on the material is given by the study of the sample surface.

Atomic Force Microscopy. The morphology of the deposited PbI_2 layers,compared to that of the TiO_2 substrate, has been monitored by Atomic Force Microscopy. In order to give representative parameters, statistics on the AFM images were carried out over different areas of the same sample and on five different samples.

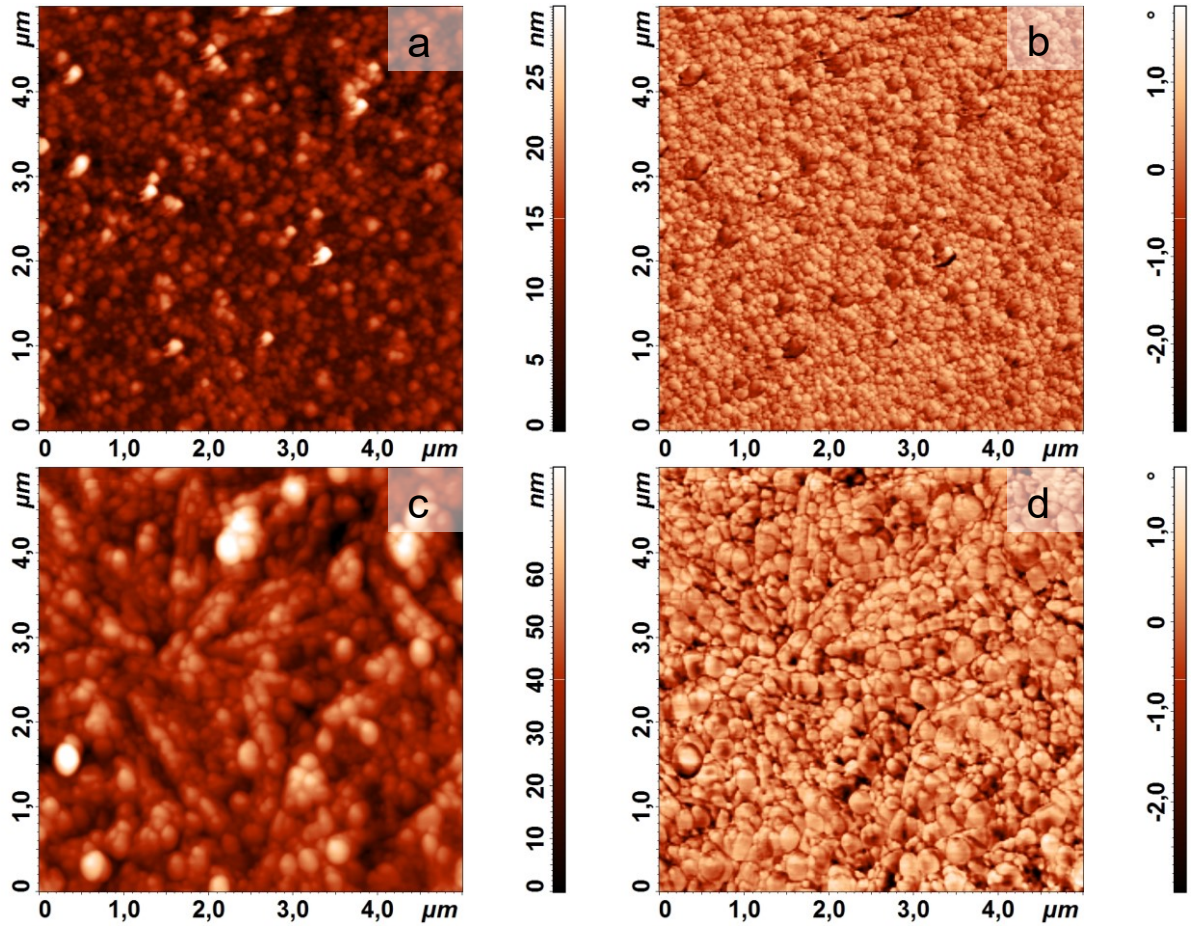

Fig 2- Height and phase AFM images of (a, b) TiO_2; (c, d) PbI_2.

The AFM height and phase images, related to the TiO_2 substrate, are shown in Fig 2-a and 2-b, respectively. As evidenced by the images, the TiO_2 layer consists of nano-sized domains homogenously distributed all over the surface. The morphological parameters disclose an average

height of ~10 nm [34,35] and an average roughness of ~2.7 nm [root mean square (RMS) roughness of ~3.6 nm], very close to what indicated by the XRR data. After the process of the PbI_2 deposition, the morphology of the sample appears modified. As evidenced by the height and the phase images of fig 2-c and 2-d, the layer shows a granular habit with a uniform distribution of the PbI_2 grains all over the TiO_2surface. The PbI_2 surface is characterized by the presence of round-shaped particles bigger than those of TiO_2. The PbI_2 grains are very often connected within each other to form some aligned rod-like structures. The value of the average height and that of the average roughness result increased with respect to the substrate, being ~35.8 nm and ~8.7 nm (RMS ~11.4 nm), respectively. The nm- thickness and the uniform morphology of the PbI_2 layers revealed, respectively, by XRR and AFM measurements, allow us appropriately monitoring the interaction at the interface between MAI and the PbI_2 film with a high control of the parameters of the interacting parts.

Uv-vis measurements. In order to characterize the optical properties of the samples, absorption measurements have been performed. Figure 3 shows the visible spectra in the range between 350 and 850 nm of the TiO_2 sample (—) before and after (—) the deposition of PbI_2 (see also the spectra after the subtraction of the TiO_2 contribution in fig S1 in S.I.).

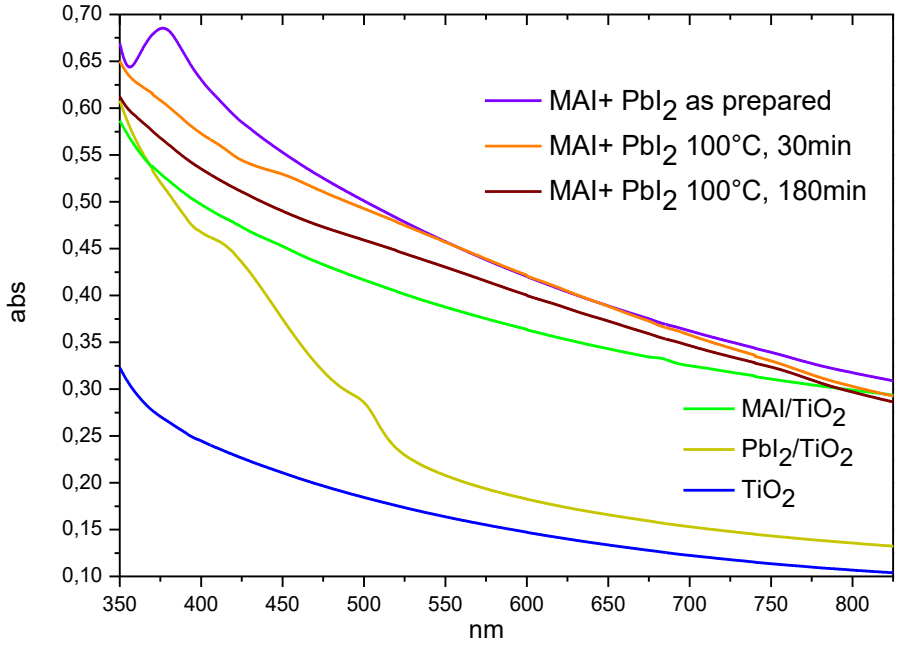

Fig 3 Transmittance spectra related to (—)TiO_2, (—)PbI_2/TiO_2; (—)MAI/TiO_2; (—)layer after MAI ($5x10^{-2}$M)+PbI_2 reaction; sample (—) after (—)30 min and (—)180 min of annealing at 100°C

Due to scattering phenomena from the surface, the optical spectrum of the annealed TiO_2 sample (—) shows a progressive variation of the absorption intensity as a function of the wavelengths with no distinctive features. Higher temperature of annealing (e.g. 500°C) are needed, in fact, to clearly observe the absorption threshold in proximity of the optical energy gap of the TiO_2 anatase polymorphism (~3.2 eV, 387 nm).[35,36]

The deposition of PbI_2 on the TiO_2 substrate leads to significant variations in the spectrum, as shown in figure 3 (—). The enhancement of the optical background is reasonably due to the increased scattering from the PbI_2 surface as the result of the higher roughness of the layer compared to that of the TiO_2 underlayer, indicated by both the AFM and XRR analyses. As can be noticed, in addition, the spectrum of the sample shows the typical optical features of the PbI_2 semiconductor, with a maximum of absorption around λ=520 nm, associated with the transition between the quasi-atomic Pb*5d* states of the PbI_2 valence band and the bottom of the conduction band having a strong Pb*6s* character. [28]

X-ray Diffraction. X-ray diffraction (XRD) measurements were performed on the PbI_2 layers in order to analyze the crystallographic structure of the material. The measurements have been carried out adopting the symmetric configuration of analysis (Bragg), so that the planes detected are those lying parallel with respect to the surface sample.

The XRD pattern of the PbI_2/TiO_2 layer is shown in figure 4a (—). As visible, a very intense peak, positioned at 2θ=12.64°, is present in the diffraction pattern, accompanied by less intense signals at 25.48°, 38.67° and 52.34° (see figure S2 in S.I.) The observed peaks arise from the (00l) family of planes of the PbI_2 lattice,[37] thus indicating a preferential growth of the layer along the direction of

the c-axis, as generally expected for systems grown into the hexagonal symmetry.[38] The orientation of the film along the c-axis is evidenced by the rocking curve (rc) shown in the right panel of figure 4 (—). The curve shows a Gaussian-like shape with a maximum centered at θ ≈ 6.2°, that is only ~0.13° off axis with respect to the normal to the sample surface. The full-width at half-maximum (FWHM) of the curve is ~4.6°, thus suggesting that the film is mainly constituted by (00l) oriented domains arranged with an angular spread of ±2-3° around the growth direction. An average PbI_2 domain size of ~23±2 nm was estimated from the FWHM of the signal at 12.64°, by applying the Scherrer's equation.[39,40]

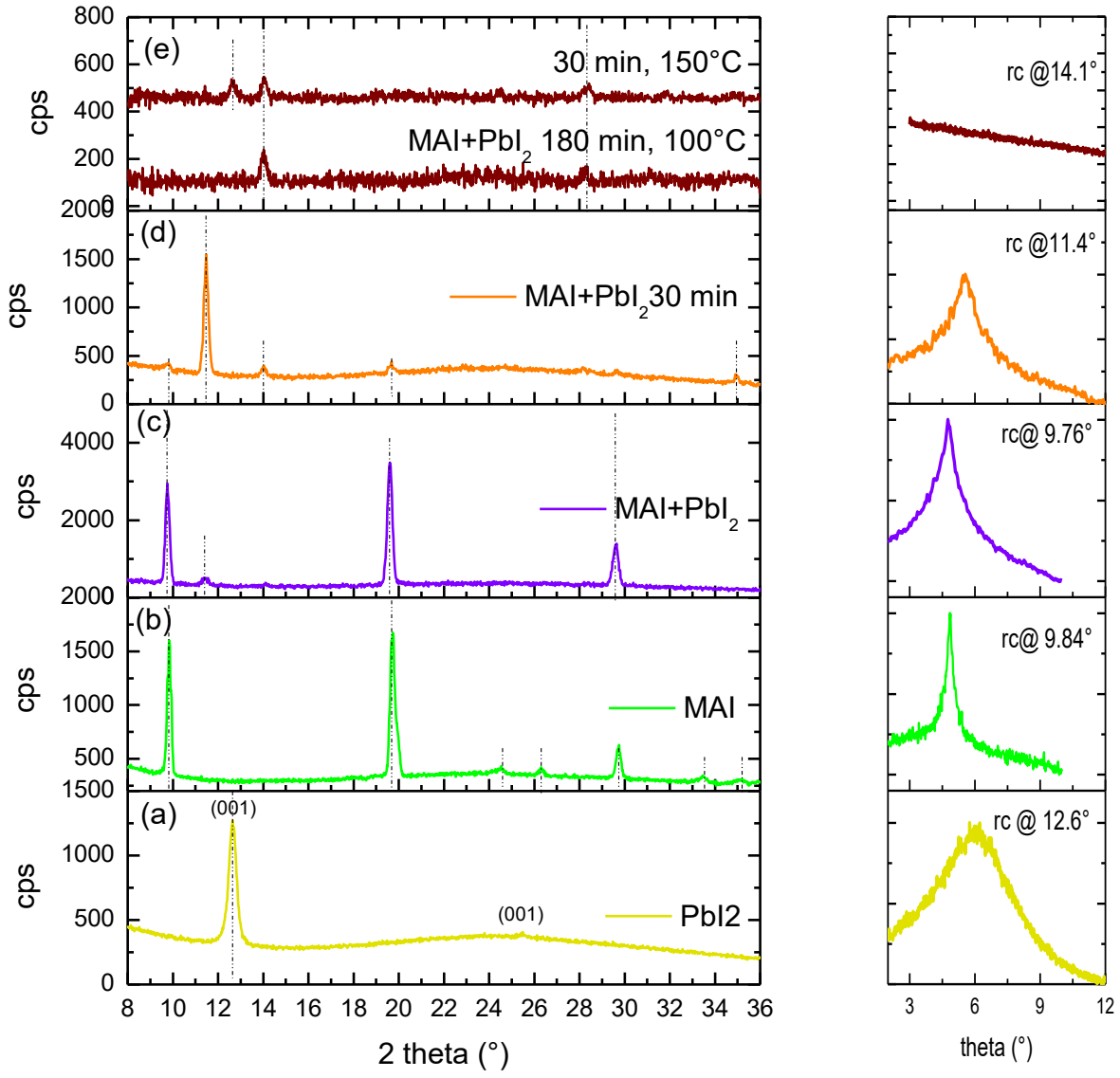

Figure 4- XRD symmetric diffraction (left panel) and rocking curve (right panel) of a) (—)PbI_2;b) (—)MAI / TiO_2 reference; c) (—)MAI + PbI_2 sample; d)(—)MAI + PbI_2 sample after 30 min of annealing; e) (—) MAI + PbI_2 sample after 180 min of annealing.

Study of the MAI+PbI_2 early interaction

The chemical reaction between the PbI_2 layer and MAI ($5x10^{-2}$M isopropyl alcoholic solution) leads to a rapid change of the color from yellow to dark brown, visible at the naked eye. In the UV-vis spectra of Figure 3, the optical characterization of the as obtained layer (—), evidences the loss of the band at 520 nm compared to PbI_2 (—) with the appearance of a new maximum at ~375 nm (blue shift), and the presence of a large absorption in a wide range of the visible spectrum (see also figure S1in S.I.).

In order to better understand the observed optical variations, absorption measurements were also performed in absence of the PbI_2 actor, on a MAI/TiO_2 reference sample, as attained by simply dipping the bare TiO_2 layer in the MAI solution.

The related UV-vis spectrum is shown in figure 3 (—). It presents a gradual increase of the optical background if compared to that of the TiO_2 substrate, but no characteristic absorption features are detected along the nanometer scale.

On the strength of this comparison, we can assert that the large visible absorption and the near-UV band at ~375 nm observed in the spectrum of the as obtained PbI_2 layer dipped with MAI (—), are reasonably due to the early interaction between the methyl-ammonium iodide and the lead iodide precursors, very similar to what observed by Stampecloskie et al., due to the complexation between PbI_2 and iodide ions.[41]

With the aim to give a further explanation of the optical results, structural investigations were performed on the samples as prepared by MAI addition (MAI+PbI_2) and also after thermal treatments.

With the interaction between the PbI_2 host layer and the MAI ($5x10^{-2}$ M isopropyl alcoholic solution), the XRD pattern of the sample (—in fig 4-c) shows notable variations if compared to the starting PbI_2 material (—). In particular, three intense signals are detected along the angular scale, respectively positioned at 2θ=9.76°, 19.66° and 29.66°. By applying the Scherrer equation to the signal lying at 2θ=9.76°, an average domain size of ~40±2 nm has been found. Note that the contribution associated with PbI_2 is no longer present in the XRD pattern; moreover, a less intense peak at 2θ=11.45° is detected after MAI addition.

Interestingly, as emerges from the comparison between the diffraction patterns of the as obtained layer (—) and that of the MAI/TiO_2 reference (fig 4b —), the three intense diffraction peaks are unequivocally associated with the (00l) family planes (multiple orders) of the MAI phase.[42] The detection of such contributions in figure 4c (—), likely indicates the presence of a layer of MAI in the sample, although further considerations are needed to better elucidate the XRD data, as it follows.

As demonstrated by the rocking curve analyses, both the MAI+PbI_2 sample and the MAI/TiO_2 reference show a marked orientation along the c-axis of the MAI lattice. In both the cases, in fact, the rocking curves acquired at 2θ ~9.8°, present a Lorentzian shape with a distinctive maximum and a narrow FWHM (see the right panel of figure 4).

In this respect, the presence of the (00l) diffraction series in the XRD pattern of the MAI +PbI_2 (—) clearly demonstrates that the formation of the layer occurs following a strongly oriented texture. In particular, the rocking curve acquired at 2θ=9.76° shows a maximum at θ=4.79° (off-axis ~0.08°) and a FWHM as narrow as ~1.3° which denotes a very close distribution of the oriented planes around the unique growth direction (see the right panel of figure 3).The occurrence of a highly-ordered layer is the result of the combination between the MAI reagents with the PbI_2 host layer. As a difference, with respect to the MAI +PbI_2 (fig 4c —), the XRD pattern of the MAI/TiO_2 reference (fig 4b —) shows the presence of other orientations different from the dominant (00l) contributions, as indicated by the additional diffraction signals along the angular scale (2θ=24.46°, 26.38°,

33.46°and 35.16°) and by the notable asymmetry of the peak at~ 19.7° found in the reference pattern (see details in figure S3 reported in S.I.). Additionally, the 2θ positions of the (00l) peaks found in the XRD pattern of the MAI +PbI_2 appear shifted towards lower angular values (higher d) if compared to those found in the pattern of the reference (see again fig S3 in S.I.). Specifically, the interplanar distance associated with the peak at the lowest 2θ value in the two diffraction patterns, results d=8.98 Å (2θ =9.84°) in the case of MAI in the reference (—) and d=9.04Å (2θ =9.76°) in that of the as obtained layer (—), thus showing a discrepancy of ~0.67%.

The peculiar structural characteristics revealed by the XRD analyses (lack of the PbI_2 signal in the pattern, strong orientation of the film and the shift of the lattice parameters), together with the optical features found by UV-vis spectroscopy (namely the band at 375 nm, not observed in the MAI/TiO_2), are indications of some chemical/ structural changes regarding the MAI lattice due to the interaction between MAI and the PbI_2. On the basis of our findings, we argue the occurrence of a phase mainly constituted by MAI-rich domains which include the exfoliated sheets of the initial lead iodide network (see scheme 1).

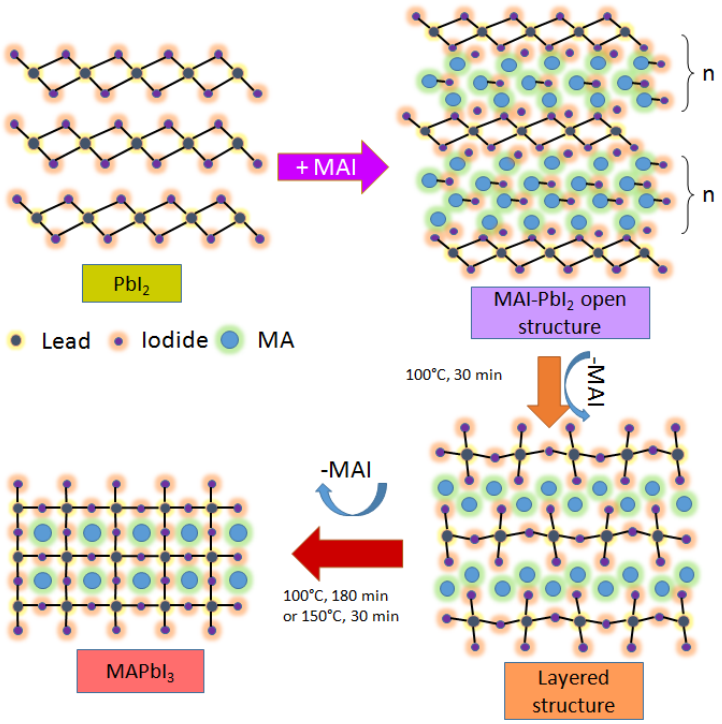

Scheme 1

This can be regarded as the 2D-layered arrangement of the PbI_2 modified by the strong mass action provided by the organic iodide precursor with the dipping of the PbI_2 layer into the MAI solution. A similar self-organization of hybrid layered compounds, originated from the intercalation of R-NH_3^+ into the parent PbI_2, was already reported by several authors.[29,43,44 -46] According to such literature, our structural data are coherent with a similar opening of the hexagonal PbI_2 oriented structure along the weakly-bonded Pb-I sheets (chemical exfoliation) with the insertion of methyl-ammonium and iodide species between the inorganic layers (see scheme 1). This produces the separation of the inorganic PbI-based foils due to MAI insertion.

Study of thermally-induced structural modification of MAI+PbI_2 layer

In order to investigate the structural modification induced by thermal process, we followed the evolution of the as-prepared MAI+ PbI_2 layer by carrying out a mild annealing at 100°C for 30 min in N_2 (fig 4-d ▬).

The XRD pattern of the sample after the annealing shows a decrease of the MAI contribution and a significant increase of the signal at 2θ=11.45°(d=7.72Å), with an associated small peak visible at higher angular values (2θ=34.9°), which is due to multiple diffraction order with n=3 (d=2.57Å). Low-intense peaks at 2θ=14.04° and 2θ=28.24°, related to the (110)/(001) and (220)/(002) planes of the tetragonal $MAPbI_3$ system, are also visible.[47]

According to the Scherrer formula applied to the dominant peak at 2θ=11.45°, the average domain size after the annealing is 36±2 nm, slightly diminished with respect to what seen for the as-prepared sample. In addition, we observed that also the planes associated with the 11.45° peak are extremely oriented, showing a narrow rocking curve centered at θ=5.8° (off-axis ~0.08°) and a FWHM of ~1.4° (see the right panel of figure 4 ▬).

On the basis of the XRD results, we argue that the phase conversion occurring at 100°C can be ascribable to the removal of MAI species as depicted in scheme 1, as further supported by the volatility of the MA and HI species [32,48](see scheme 1).

The structural modification triggered by the thermal treatment is reasonably accompanied by the re-arrangement of the structure of the connected PbI_6 units along the extended inorganic network. [28] Previous literature on two-dimensional lattices formed from a simple intercalation of RNH_3^+ into the PbI_2 sheets indicates that similar hybrid structures have the generic structural formula of $(RNH_3)_2PbI_4$. [17,43-**Errore. Il segnalibro non è definito.**[46, 49,50] The organic/inorganic alternate stacking is organized with a high degree of orientation (very similarly to our case) by attractive ionic interactions between the RNH_3^+ and PbI_6^{4-}, whilst van der Waals interactions occur within the organic chains of the molecular layer (spacer). This confines the perovskite in bi-dimensionality because of steric effects. In this 2-D structures, the four equatorial iodides (bridging iodides) are shared, whilst the two axial iodides (terminal iodides) are unshared, as suggested by Billing et al. [27] for a 2-D structure formed by $(C_nH_{2n+1}NH_3)_2PbI_4$](n = 12, 14, 16 and 18) and by Mitzi in the case of well-defined 2D layers [26](scheme 2).

On this literature basis, we propose that the octahedral halide coordination around the lead, shows a different sharing and tilting of the connected [PbI_6] units with respect to the parent PbI_2 lattice, due to the higher number of iodine ions per Pb^{2+}.The resulting negative charges of the octahedral units are balanced by the cationic MA^+ moieties. The presence of a dominant peak at 11.45° is, in our opinion, due to the formation of this layered structure. Note, that in literature the attribution of the peak lying at 11.45° is not univocal. It has been associated with the bi-hydrate phase of the $MAPbI_3$ structure having formula $MA_4PbI_6{\cdot}2H_2O$, [23,51,52] as well to a low-dimensional perovskite phase with formula MA_4PbI_6.[53] Please note that hydrate perovskites are claimed to be formed under specific experimental conditions, with humidity percentage around 80%. Instead, we performed the thermal process under inert environment (N_2). Certainly, such a peak, found in the XRD pattern of the sample after the annealing for 30 min at 100°C, cannot be attributed either to MAI or to PbI_2 but, conversely, it can be associated with an intermediate phase produced by the combination between the two organic and inorganic precursors. This is of significance, further demonstrating the presence of some lead-iodide “seeds” incorporated in the MAI-rich phase of the as-obtained layer. The

interpretation of our data is that the gradual loss of MAI induced by the thermal treatment has favored a better reorganization of the different ionic species with the formation of a layered organic/ inorganic network, indeed characterized by the peak at 11.45°.

As described in our previous work,[54] in strict accordance with what hereto discussed, the presence of an intermediate phase (peak at 11.5°) was found in the XRD pattern of a sample obtained by spin-coating from a single synthetic step by using a non-stoichiometric 1PbI_2: 3MAI ratio (I/Pb=5/1, iodide excess), consistently with what reported by Yan et al.[55]

Conversely, no intermediates were observed in the case of the 1MAI:1PbI_2 preparation, thus indicating the role played by the stoichiometric ratio in affecting the mechanism of formation of the phase.

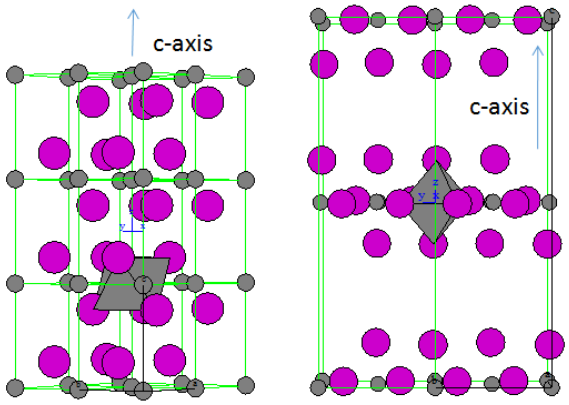

Scheme 2 (the 2D structure has been built according to the atomic parameters of ref 26)

The structural re-organization of the lattice triggered by the thermal budget is, correspondingly, envisioned by optical analyses which shows significant optical changes (Fig. 3 and S1 —), indicating the occurrence of a chemical/structural modification which promotes a different accomplishment of the energy levels.[32]

The establishment of dominant $MAPbI_3$ phase in the XRD pattern is achieved by prolonging the annealing at 100°C to 180 min (— in fig 4-e). In this case, in fact, the XRD pattern shows just the expected contributions originated from the perovskite *I4/mcm* tetragonal system, with the

typical 14.06° and 28.30° peaks and a small contribution at 31.84° due to the (310) planes. According to the Scherrer formula, the average domain size, as evaluated from the 14.06° peak, is ~32.0 nm. Similar results are achieved after 30 min of annealing at 150°C.[54] In the latter case, the presence of PbI_2 in the pattern is also observed, but rather generated from the instability of the perovskite structure at that temperature.[56]

Consistently with the XRD results, the optical characterization of the sample annealed for 180 min for 30 min (figure 3 and S1 —), reveals the presence of the $MAPbI_3$ phase, diagnostically characterized by an edge of absorption at λ=796 nm. Such wavelength value corresponds, in fact, to the perovskite band gap (~1.56 eV), in perfect accordance with the literature data.[57]

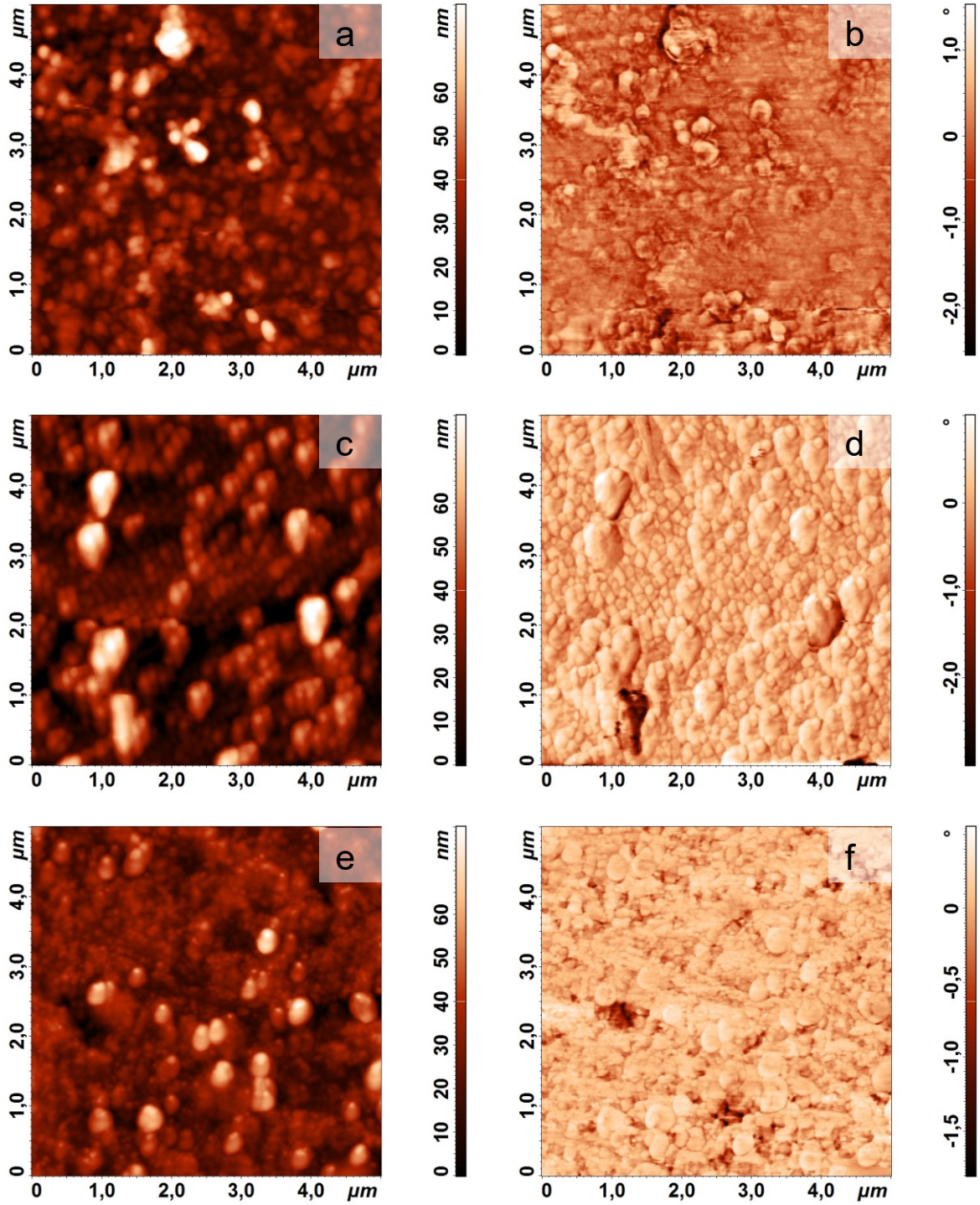

Fig 5. Height and phase AFM images (a,b) MAI + PbI_2 sample, (c,d)MAI ($5x10^{-5}$M)/ PbI_2 after 120 min and (e,f) 180 minutes of annealing at 100C.

To evaluate the effect of the thermal annealing on the sample morphology, AFM analyses were carried out. After the analysis performed on the as-obtained MAI+PbI_2 layer (figure 5 a-b, average height ~30 nm and RMS 11.7 nm), the morphological measurements conducted on the 30 min-annealed sample (figure 5 c-d) reveal that the surface is characterized by the presence of some organized features standing on the surface, having an average height of ~33.0 nm and RMS ~ 7.5 nm, consistently with the X-ray results obtained by Scherrer equation. Similarly, the morphology of the 180min-annealed sample shows the presence of high domains on the surface (fg 5 e-f),with an average height of ~28.5 nm and a RMS value of ~7.2 nm, as estimated statistically.

Effect of MAI concentration on MA-Pb-I layers

In order to confirm the role of the MAI species in the formation of the layered hybrid MA-Pb-I structure, we tuned the amount of MAI in the solution. In particular, the concentration of MAI was reduced by 1/5 and by 1/100 with respect to the $5x10^{-2}$M hereto discussed, specifically, achieving $1x10^{-2}$M and $5x10^{-4}$M.

For the sake of simplicity, the diffraction data are presented in the diagnostic angular range reduced from 2θ =8 to 15° in figure 6. The use of the most dilute solution does not appreciably modify the diffraction pattern with respect to that of the starting PbI_2 host layer. The XRD pattern (fig 6-a), in fact, shows only the peak at 12.64° related to the (001) planes of the PbI_2, thus indicating that the negligible amount of MAI present in solution is not sufficient to alter the PbI_2 architecture.

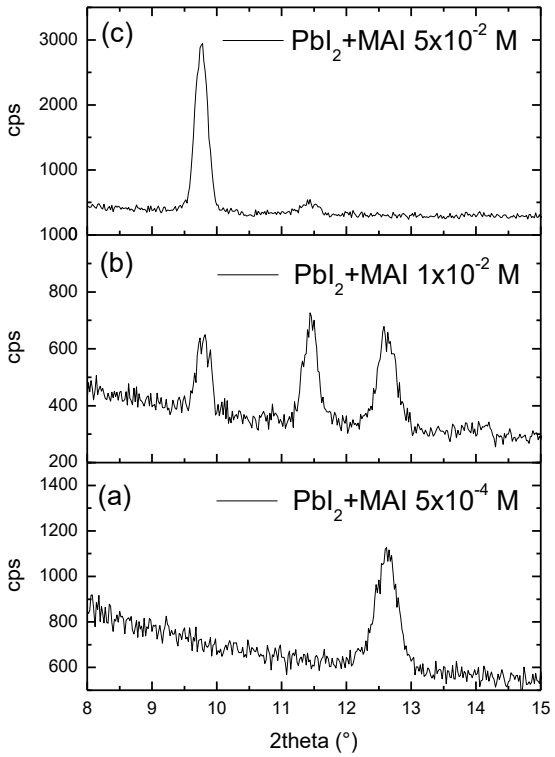

Figure 6- XRD symmetric diffraction patterns of samples obtained from (a) 5x10^{-4} M, (b) 1x10^{-2}M and (c) 5x10^{-2} M MAI solutions.

On the other hand, the X-ray pattern of the sample as obtained from the 1x10^{-2}M solution (fig 6-b), shows the presence of a mixture of phases, including the unreacted PbI_2. This multi-faceted scenario indicates that the relative amount of the hybrid phases obtained is a function of the MAI content present in the solution and interacting with PbI_2. As already discussed, at high MAI concentration, due to a more effective mass action, the PbI_2 layer is completely integrated in the MAI-rich ordered matrix (fig 6-c).

CONCLUSION

The paper describes the structural modifications occurring in the PbI_2 hexagonal structure as a consequence of the interaction with MAI, starting from their early stages, according to the two-step method used for the synthesis of perovskites. To this intent, a uniform and thin PbI_2 layer (20±5 nm), grown oriented along the *c*-axis on low-rough TiO_2 substrate was used to reproduce the interaction at the interface between the MAI solution (with different concentrations) and the surface of PbI2. At high MAI concentration, the combination between PbI_2 with MAI leads to the formation of self-organized highly oriented system consisting in a MAI-rich phase with inorganic Pb-I frameworks included. This occurs through the opening of the PbI_2 hexagonal structure (chemical exfoliation) due to the methyl-ammonium intercalation together with the re-arrangement of the octahedral PbI_6^{2-} units in the inorganic structure (different sharing and tilting with respect to PbI_2). This intermediate phase, being in excess of MA^+ and iodide species, keeps the orientation of the starting PbI_2 layer and is diagnostically characterized by a peak at 2θ=11.45°. Consistently, the formation of the intermediate phase with the XRD peak at 11.45° was observed also in the case of a film obtained by spin-coating from a 3MAI:1 PbI_2 single-step synthetic route after annealing at 100°C.[54] In the same work, no intermediates were observed in the same conditions for the 1MAI:1PbI_2 preparation, thus, further indicating that the MAI/PbI_2 ratio plays a fundamental role in affecting the formation mechanism of the phase.

Due to the volatility of the organic part, the metastable intermediate phase can convert into the $MAPbI_3$ I4/mcm structure by thermal annealing. The structural modifications revealed by XRD are, consistently, accompanied by variations of the optical properties (UV-vis). The as-obtained sample shows a large absorption in the visible range and a near-UV band at 375 nm. In particular, the annealing at 100°C leads to the strong decrease of the near-UV contribution, whilst the broad visible absorption results enhanced and red-shifted. In agreement with the literature, the formation

of the 3D $MAPbI_3$perovskite is evidenced by a further red-shift and by the optical band gap around λ=796 nm (1.56 eV).

The paper indeed gives various insights (structural, optical) on the mechanism of formation of the MAPbI3 structure from the early interaction at the interface between the two MAI and PbI2 precursors and the formation of a layered MA-Pb-I intermediate in regime of high MAI content. We think that this behavior should be of interest for the scientific community working on the perovskite growth and should be taken into account in the set up of the synthesis procedure. To take advantage also in thick films growth, the MAI diffusion (along the thickness) and its intercalation into the host PbI2 layer must be tightly controlled before reaction. We indeed believe that parameters such the PbI2 thickness and its texture, the MAI concentration and the PbI2 dipping time in the MAI solution, since mutually correlated, are crucial on the dynamics of hybrid phases formation trough intercalation and, in turns, also on the texture and quality of the final MAPbI3 architecture.

For all these reasons, we believe that our understanding can contribute to further rationalize the perovskite growth and to design the properties of the final material.

SUPPORTING INFORMATION AVAILABLE: Figure S1: UV-vis spectra obtained by subtracting the TiO_2 contribution from the PbI_2/TiO_2; MAI/TiO_2; layer after MAI ($5x10^{-2}$M)+PbI_2 reaction and after 30 min and 180 min of annealing at 100°C data; Figure S2: Long range X-ray Diffraction pattern of PbI_2 deposited on the TiO_2 substrate. Figure S3: Comparison between the X-ray Diffraction patterns of MAI respectively on the PbI_2 /TiO_2 and MAI/TiO_2 samples in the diagnostic angular range of the (00l) MAI planes.

ACKNOWLEDGMENTS: This work was supported by the CNR Italian project EFOR-CABIR (CUP B51J10001290001).

[1] Gao, P.; Grätzel, M.; Nazeeruddin, M. K. Environmental Science Organohalide Lead Perovskites for Photovoltaic Applications.**2014**, *1* (c), 2448–2463.

[2] K.-L.Wu, A. Kogo, N.Sakai, M. Ikegami, T. Miyasaka, High efficiency and robust performance of organo lead perovskite solar cells with large grain absorbers prepared in ambient air conditions. Chem. Lett., **2015**, *44*,321-323,

[3] Kojima, A.; Teshima, K.; Shirai, Y.; Miyasaka, T. Organometal Halide Perovskites as Visible-Light Sensitizers for Photovoltaic Cells. *J. Am. Chem. Soc.***2009**, *131* (17), 6050–6051.

[4] Collavini, S.; Völker, S. F.; Delgado, J. L. Understanding the Outstanding Power Conversion Efficiency of Perovskite Based Solar Cells. *Angew. Chemie Int. Ed.***2015**, 54, 9757-9759.

[5] Tan, Z.-K.; Moghaddam, R. S.; Lai, M. L.; Docampo, P.; Higler, R.; Deschler, F.; Price, M.; Sadhanala, A.; Pazos, L. M.; Credgington, D.; et al. SI: Bright Light-Emitting Diodes Based on Organometal Halide Perovskite. *Nat. Nanotechnol.***2014**, *9*, 687–692.

[6] Hoye, R. L. Z.; Chua, M. R.; Musselman, K. P.; Li, G.; Lai, M. L.; Tan, Z. K.; Greenham, N. C.; MacManus-Driscoll, J. L.; Friend, R. H.; Credgington, D. Enhanced Performance in Fluorene-Free Organometal Halide Perovskite Light-Emitting Diodes Using Tunable, Low Electron Affinity Oxide Electron Injectors. *Adv. Mater.***2015**, *27* (8), 1414–1419.

[7] Wang, J.; Wang, N.; Jin, Y.; Si, J.; Tan, Z. K.; Du, H.; Cheng, L.; Dai, X.; Bai, S.; He, H.; et al. Interfacial Control toward Efficient and Low-Voltage Perovskite Light-Emitting Diodes. *Adv. Mater.***2015**, *27* (14), 2311–2316.

[8]Sadhanala, A.; Kumar, A.; Pathak, S.; Rao, A.; Steiner, U.; Greenham, N. C.; Snaith, H. J.; Friend, R. H. Electroluminescence from Organometallic Lead Halide Perovskite-Conjugated Polymer Diodes. *Adv. Electron. Mater.***2015**,1,1500008 (1-5)

[9]Snaith, H. J. Perovskites : The Emergence of a New Era for Low-Cost , High-. *J. Phys. Chem. Lett* **2013**, *4*, 3623−3630.

[10]Stranks, S. D.; Stranks, S. D.; Eperon, G. E.; Grancini, G.; Menelaou, C.; Alcocer, M. J. P.; Leijtens, T.; Herz, L. M.; Petrozza, A.; Snaith, H. J. Electron-Hole Diffusion Lengths Exceeding. **2014**, *341* (2013), 341–345.

[11]Eperon, G. E.; Stranks, S. D.; Menelaou, C.; Johnston, M. B.; Herz, L. M.; Snaith, H. J. Supplementary Information Formamidinium of Formamidinium Lead Trihalide: A Broadly Tunable Perovskite for Efficient Planar Heterojunction Solar Cells. *Energy Environ. Sci.***2014**, *7* (3), 982-988.

[12] Noh, J. H.; Im, S. H.; Heo, J. H.; Mandal, T. N.; Seok, S. Il. Chemical Management for Colorful, Efficient, and Stable Inorganic-Organic Hybrid Nanostructured Solar Cells. *Nano Lett.***2013**, *13* (4), 1764–1769.

[13] Sum, T. C.; Mathews, N. Advancements in Perovskite Solar Cells: Photophysics behind the Photovoltaics. *Energy Environ. Sci.***2014**, 2518–2534.

[14] Even, J.; Pedesseau, L.; Katan, C.; Kepenekian, M.; Lauret, J. S.; Sapori, D.; Deleporte, E. Solid-State Physics Perspective on Hybrid Perovskite Semiconductors. *J. Phys. Chem. C***2015**, *119* (19), 10161–10177.

[15]Guo, L.; Sun, Z.; Zhao, G.; Li, X.; Liu, H. Synthesis and Characterization of Layered Perovskite-Type Organic-Inorganic hybrids(R-NH3)2(CH3NH3)Pb 2I7. *J. Wuhan Univ. Technol. Mater. Sci. Ed.***2012**, *27* (5), 957–961.

[16] Tanaka, K.; Kondo, T. Bandgap and Exciton Binding Energies in Lead-Iodide-Based Natural Quantum-Well Crystals. *Sci. Technol. Adv. Mater.***2003**, *4* (6), 599–604.

[17] Cao, D. H.; Stoumpos, C. C.; Farha, O. K.; Hupp, J. T.; Kanatzidis, M. G. 2D Homologous Perovskites as Light-Absorbing Materials for Solar Cell Applications. *J. Am. Chem. Soc.***2015**, *137* (24), 7843–7850.

[18]Kawamura, Y.; Mashiyama, H.; Hasebe, K. Structural Study on Cubic−Tetragonal Transition of CH3NH3PbI3.*J. Phys. Soc. Jpn.* **2002**, 71, 1694−1697.

[19]Ko, H.-S.; Lee, J.-W.; Park, N.-G. 15.76% Efficiency Perovskite Solar Cells Prepared under High Relative Humidity: Importance of PbI2 Morphology in Two-Step Deposition of CH3NH3PbI3. *J. Mater. Chem. A* **2015**, *3 (16)*, 8808−8815.

[20] Wu, C.-G.; Chiang, C.-H.; Tseng, Z.-L.; Nazeeruddin, M. K.; Hagfeldt, A.; Grätzel, M. High Efficiency Stable Inverted Perovskite Solar Cells without Current Hysteresis. *Energy Environ. Sci.* **2015**, *8 (9)*, 2725−2733.

[21] Gong, X.; Li, M.; Shi, X.-B.; Ma, H.; Wang, Z.-K.; Liao, L.-S. Controllable Perovskite Crystallization by Water Additive for High- Performance Solar Cells. *Adv. Funct. Mater.* **2015**, *25 (42)*, 6671− 6678.

[22]Ahn, N.; Son, D.-Y.; Jang, I.-H.; Kang, S. M.; Choi, M.; Park, N.- G. Highly Reproducible Perovskite Solar Cells with Average Efficiency of 18.3% and Best Efficiency of 19.7% Fabricated via Lewis Base Adduct of Lead(II) Iodide. *J. Am. Chem. Soc.* **2015**, *137 (27)*, 8696− 8699.

[23] Patel, J. B.; Milot, R. L.; Wright, A. D.; Herz, L. M.; Johnston, M. B. Formation Dynamics of CH 3 NH 3 PbI 3 Perovskite Following Two-Step Layer Deposition. *J. Phys. Chem. Lett.***2015**, *7* (1), 96−102

[24] Even, J.; Pedesseau, L.; Katan, C.; Kepenekian, M.; Lauret, J. S.; Sapori, D.; Deleporte, E. Solid-State Physics Perspective on Hybrid Perovskite Semiconductors. *J. Phys. Chem. C***2015**, *119* (19), 10161–10177.

[25] Cheng, Z.; Lin, J. Layered Organic–inorganic Hybrid Perovskites: Structure, Optical Properties, Film Preparation, Patterning and Templating Engineering. *CrystEngComm* **2010**, *12* (10), 2646.

[26] Mitzi, D. B. Synthesis, Crystal Structure, and Optical and Thermal Properties of $(C_4H_9NH_3)_{(2)}MI_{(4)}$ (M=Ge, Sn, Pb). *Chem. Mater.***1996**, *8* (3), 791–800.

[27] Billing, D. G.; Lemmerer, A. Synthesis, Characterization and Phase Transitions of the Inorganic–organic Layered Perovskite-Type Hybrids $[(C_nH_{2n+1}NH_3)2PbI_4]$(n = 12, 14, 16 and 18). *New J. Chem.***2008**, *32*, 1736–1746.

[28]T.Ishihara, Proceedings of the international school of Physics Enrico Fermi, Ios press, Amsterdam 2002, DOI 10.3254/1-58603-271-2-491

[29]Liang, K.; Mitzi, D. B.; Prikas, M. T. Synthesis and Characterization of Organic - Inorganic Perovskite Thin Films Prepared Using a Versatile Two-Step Dipping Technique.*Chem. Mater.***1998**, *10* (8), 403–411.

[30] Mercier, N. $(HO_2C(CH_2)_3NH_3)_2(CH_3NH_3)Pb_2I_7$: A Predicted Non-Centrosymmetrical Structure Built up from Carboxylic Acid SupramolecularSynthons and Bilayer Perovskite Sheets. *CrystEngComm* **2005**, *7* (70), 429.

[31] I. Deretzis, I.; Di Mauro, B.N.; Alberti, A.; Pellegrino, G.; Smecca, E.; La Magna, A. Spontaneous bidirectional ordering of CH3NH3+ in lead iodide perovskites at room temperature: The origins of the tetragonal phase. *Sci Rep.* **2016**, 6, 24443

[32] Jain, S. M.; Philippe, B.; Johansson, E. M. J.; Park, B.; Rensmo, H.; Edvinsson, T.; Boschloo, G. Vapor Phase Conversion of PbI_2 to $CH_3NH_3PbI_3$: Spectroscopic Evidence for Formation of an Intermediate Phase. *J. Mater. Chem. A,* **2016***,4,* 2630-2642.

[33] Pellegrino, G.; Alberti, A.; Condorelli, G. G.; Giannazzo, F.; Magna, A. La; Paoletti, A. M.; Pennesi, G.; Rossi, G.; Zanotti, G. Study of the Anchoring Process of Tethered Unsymmetrical Zn-Phthalocyanines on TiO 2 Nanostructured Thin Films. *J. Phys. Chem. C* **2013**, *117*, 11176–11185.

[34] Pellegrino, G.; Bongiorno, C.; Ravesi, S.; Alberti, A. Thin Films Deposited at 150 °C by Dc-Reactive Sputtering on Fiber-Textured [0 0 0 1] ZnO : Al Substrates. *J. Phys. D. Appl. Phys.* **2012**, *45* (35), 355301.

[35]Alberti, A.; Bongiorno, C.; Pellegrino, G. Anatase/Rutile Nucleation and Growth on (0002) and (11-20) Oriented ZnO:Al/glass Substrates at 150 C. *Thin Solid Films***2014**, *555*, 3–8.

[36] Pellegrino, G.; Condorelli, G. G.; De Rossi, F.; Brown, T. M.; Giovenale, F.; Bongiorno, C.; Alberti, A. Thermally Induced Structural Modifications of Nano-Sized Anatase Films and the Effects on the Dye-TiO2 Surface Interactions. *Appl. Surf. Sci.***2014**, *296*, 69–78.

[37]ZhiZheng, Airuo Liu, ShuminWang,Yu Wang, ZhaoshengLi,Woon Ming Lau and Lizhi Zhang. Mater. Chem. In situ growth of epitaxial lead iodide films composed of hexagonal single crystals. **2005**,*15*, 4555–4559

[38] Alberti, A.; Deretzis, I.; Pellegrino, G.; Bongiorno, C.; Smecca, E.; Mannino, G.; Giannazzo, F.; Condorelli, G. G.; Sakai, N.; Miyasaka, T.; et al. Similar Structural Dynamics for the Degradation of CH3NH 3PbI3 in Air and in Vacuum. *ChemPhysChem.* **2015**, *16* (14), 3064–3071.

[39]Cullity B D 1978 Elements of X-ray Diffraction 2nd edn (Menlo Park, CA: Addison-Wesley) p 102

[40]Alberti, A.; Pellegrino, G.; Condorelli, G. G.; Bongiorno, C.; Morita, S.; La Magna, A.; Miyasaka, T. Efficiency Enhancement in ZnO:Al-Based Dye-Sensitized Solar Cells Structured with Sputtered TiO2 Blocking Layers. *J. Phys. Chem. C* **2014**, *118* (13), 6576–6585.
[41]Stamplecoskie, K. G.; Manser, J. S.; Kamat, P. V. Dual Nature of the Excited State in Organic-Inorganic Lead Halide Perovskites. *Energy Environ. Sci.* **2015**, *8* (1), 208–215.

[42] Chiang, C.-H.; Tseng, Z.-L.; Wu, C.-G. Planar Heterojunctionperovskite/PC71BM Solar Cells with Enhanced Open-Circuit Voltage via a (2/1)-Step Spin-Coating Process. *J. Mater. Chem. A* **2014**, *2*, 15897–15903

[43]Pradeesh, K.; Baumberg, J. J.; Prakash, G. V. In Situ Intercalation Strategies for Device-Quality Hybrid Inorganic-Organic Self-Assembled Quantum Wells. *Appl. Phys. Lett.***2009**, *95* (3).

[44]Gauthron, K.; Lauret, J.; Doyennette, L.; Lanty, G.; Choueiry, A. Al; Zhang, S. J.; Largeau, L.; Mauguin, O.; Bloch, J.; Deleporte, E. Optical Spectroscopy of Two-Dimensional Layered (C 6 H 5 C 2 H 4 -NH 3) 2 -PbI 4 Perovskite. **2010**, *18* (6), 5912–5919.

[45]Cheng, Z.; Lin, J. Layered Organic–inorganic Hybrid Perovskites: Structure, Optical Properties, Film Preparation, Patterning and Templating Engineering. *CrystEngComm***2010**, *12* (10), 2646.

[46]Ahmad, S.; Kanaujia, P. K.; Niu, W.; Baumberg, J. J.; Prakash, G. V.In Situ Intercalation Dynamics in Inorganic − Organic Layered Perovskite Thin Films. **2014**, 6, 10238−10247.

[47] Colella, S.; Mosconi, E.; Pellegrino, G.; Alberti, A.; Guerra, V. L. P.; Masi, S.; Listorti, A.; Rizzo, A.; Condorelli, G. G.; De Angelis, F.; et al. Elusive Presence of Chloride in Mixed Halide Perovskite Solar Cells. *J.Phys. Chem. Lett.***2014**, *5* (20), 3532–3538.

[48]Deretzis, I.; Alberti, A.; Pellegrino, G.; Smecca, E.; Giannazzo, F.; Sakai, N.; Miyasaka, T.; La Magna, A. AtomisticOrigins of $CH_3NH_3PbI_3$Degradation to PbI_2 in Vacuum. *Appl. Phys. Lett.***2015**, *106* (13).

[49] Even, J.; Pedesseau, L.; Katan, C.; Kepenekian, M.; Lauret, J. S.; Sapori, D.; Deleporte, E. Solid-State Physics Perspective on Hybrid Perovskite Semiconductors. *J. Phys. Chem. C***2015**, *119* (19), 10161–10177.

[50] Cheng, Z.; Lin, J. Layered Organic–inorganic Hybrid Perovskites: Structure, Optical Properties, Film Preparation, Patterning and Templating Engineering. *CrystEngComm* **2010**, *12* (10), 2646.

[51]Leguy, A. M. A.; Hu, Y.; Campoy-Quiles, M.; Alonso, M. I.; Weber, O. J.; Azarhoosh, P.; van Schilfgaarde, M.; Weller, M. T.; Bein, T.; Nelson, J.; et al. Reversible Hydration of $CH_3NH_3PbI_3$ in Films, Single Crystals, and Solar Cells. *Chem. Mater.***2015**, *27* (9), 3397–3407

[52]Halder, A.; Choudhury, D.; Ghosh, S.; Subbiah, A. S.; Sarkar, S. K. Exploring Thermochromic Behavior of Hydrated Hybrid Perovskites in Solar Cells. *J. Phys. Chem. Lett.***2015**, *6* (16), 3180–3184.

[53] Song, Z.; Watthage, S. C.; Phillips, A. B.; Tompkins, B. L.; Ellingson, R. J.; Heben, M. J. Impact of Processing Temperature and Composition on the Formation of Methylammonium Lead Iodide Perovskites. *Chem. Mater.***2015**, *27* (13), 4612–4619.

[54] Pellegrino, G.; Colella, S.; Deretzis, I.; Condorelli, G. G.; Smecca, E.; Gigli, G.; La Magna, A.; Alberti, A. Texture of MAPbI3 Layers Assisted by Chloride on Flat TiO2 Substrates. *J. Phys. Chem. C***2015**, 119, 19808−19816

[55] Yan, K.; Long, M.; Zhang, T.; Wei, Z.; Chen, H.; Yang, S.; Xu, J. Hybrid Halide Perovskite Solar Cell Precursors: Colloidal Chemistry and Coordination Engineering behind Device Processing for High Efficiency *J. Am. Chem. Soc.* **2015**, *137*, 4460−4468.

[56] Smecca, E.; Numata, Y.; Deretzis, I.; Pellegrino, G.; Boninelli, S.; Miyasaka, T.; La Magna, A.; Alberti, A. Stability Of Solution-Processed MAPbI3 and FaPbI3 Layers. *Physical Chemistry Chemical Physics .,* **2016***,18*, 13413-13422

[57] Lee, M. M.; Teuscher, T.; Miyasaka, T.; Murakami, T. N.; Snaith, H. J. Efficient hybrid solar cells based on meso-superstructured organometal halide perovskites. *Science,***2012***, 338* (6107) 643-647

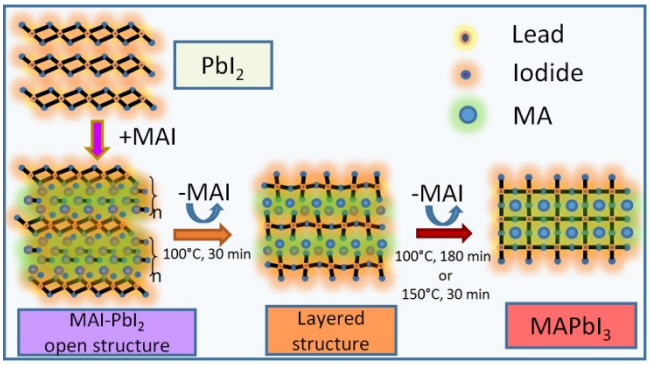

Table of Content